ARMY RESEARCH LABORATORY

Pulsed Laser Deposition of Ferroelectric Thin Films in Conjunction With Superconducting Oxides

S. Sengupta, L.C. Sengupta, J.D. Demaree, and W. Kosik

ARL-TR-654

December 1994

Approved for public release; distribution unlimited.

The findings in this report are not to be construed as an official Department of the Army position unless so designated by other authorized documents.

Citation of manufacturer's or trade names does not constitute an official endorsement or approval of the use thereof.

Destroy this report when it is no longer needed. Do not return it to the originator.

REPORT DOCUMENTATION PAGE

Form Approved
OMB No. 0704-0188

1. AGENCY USE ONLY *(Leave blank)*	2. REPORT DATE	3. REPORT TYPE AND DATES COVERED
	December 1994	

4. TITLE AND SUBTITLE
Pulsed Laser Deposition of Ferroelectric Thin Films in Conjunction with Superconducting Oxides

5. FUNDING NUMBERS

6. AUTHOR(S)
S. Sengupta, L.C. Sengupta, J.D. Demaree, and W. Kosik

7. PERFORMING ORGANIZATION NAME(S) AND ADDRESS(ES)
Army Research Laboratory
Watertown, MA 02172-0001
AMSRL-MA-CA

8. PERFORMING ORGANIZATION REPORT NUMBER
ARL-TR-654

9. SPONSORING/MONITORING AGENCY NAME(S) AND ADDRESS(ES)

10. SPONSORING/MONITORING AGENCY REPORT NUMBER

11. SUPPLEMENTARY NOTES

12a. DISTRIBUTION/AVAILABILITY STATEMENT
Approved for public release, distribution unlimited.

12b. DISTRIBUTION CODE

13. ABSTRACT *(Maximum 200 words)*

The possibility of combining ferroelectrics and superconductors has been of interest for use in memory storage devices. Additionally, superconductors offer crystal structures compatible to the epitaxial growth of the ferroelectric, $Ba_{0.6}Sr_{0.4}TiO_3$ (BSTO), which is cubic at this stoichiometry. BSTO has a lattice constant of 3.94 Å as compared to the superconducting $Pr_{2-x}Ce_xCuO_4$ tetragonal single crystal which also has a lattice constant of a=3.94 Å. (minor variations with Cerium content).

In this study, ferroelectric thin films of BSTO were deposited on single crystals of Pr_2CuO_4 and $Pr_{2-x}Ce_xCuO_4$. The optical constants of the substrates, single crystals of Pr_2CuO_4 and $Pr_{2-x}Ce_xCuO_4$ were determined using Variable Angle Spectroscopic Ellipsometry (VASE) and the composition and crystal structure were examined using Rutherford Backscattering Spectrometry (RBS) with ion beam channeling. The substrate/film interfaces and the compositional variation in the films were also studied with RBS and with SEM / EDS. Glancing angle x-ray diffraction was used to verify the epitaxial nature of the films. The effect of the deposition parameters (laser repetition rate, oxygen backfill pressure, and deposition geometry) on the quality of the films was experimented with previously and only the optimized parameters were used.

14. SUBJECT TERMS	15. NUMBER OF PAGES
PLD, Ferroelectric Films, BSTO, Superconducting Oxides	13
	16. PRICE CODE

17. SECURITY CLASSIFICATION OF REPORT	18. SECURITY CLASSIFICATION OF THIS PAGE	19. SECURITY CLASSIFICATION OF ABSTRACT	20. LIMITATION OF ABSTRACT
Unclassified	Unclassified	Unclassified	UL

Contents

Figures

Tables

INTRODUCTION

There has been a significant interest in the possibility of combining superconductors with ferroelectrics for application in memory storage devices by using the superconductors for electrodes [1]. The idea of using single crystal superconductors for substrates, however, has not been rigorously investigated. There are advantages to using these oxides as substrates. One of which is the excellent lattice match between the Barium Strontium Titanate, $Ba_{0.6}Sr_{0.4}TiO_3$, BSTO, and the crystal. Also the possibility of using the substrate itself as the bottom electrode is an attractive alternative to a metallic bottom electrode which can cause shorting [2].

In this study, the Top Seeded Solution Growth technique has been used to obtain single crystals of $Pr_{2-x}Ce_xCuO_4$ (x=0 and x=0.17). This technique, unlike other growth procedures, can produce large specimens that contain fairly uniform dopant distributions [3]. The cuprate substrates had been annealed in an attempt to decrease its resistivity. The effect of the Ce doping and annealing on the optical constants has been monitored using VASE, and the effect of both the Ce doping and annealing on the crystal structure of the substrates has been examined using RBS with ion beam channeling.

Films of $Ba_{0.6}Sr_{0.4}TiO_3$ have been deposited onto the crystals using Pulsed Laser Deposition (PLD); the films were then examined using RBS, SEM / EDS, and glancing angle x-ray diffraction. The effect of the deposition parameters on the quality of the films as measured by these analytical techniques will be discussed.

EXPERIMENTAL

The single crystal specimens had their c-axis oriented perpendicular to the crystal surface. The as-grown crystals were analyzed using the techniques mentioned above. The details of the RBS and VASE experiments analysis are given below. Both the crystals were annealed at 950 ^{0}C for about 15 hours in flowing argon. The crystals were then re-examined [4].

The PLD was accomplished using a krypton-fluoride excimer laser with a wavelength of 248 nm and a repetition rate of 10 Hz. The average pulse energy was 300 mJ. The oxygen partial pressure in the chamber was 200 mT and the substrate temperature was 520 ^{0}C . The substrate temperature was monitored by clamping the thermocouple in-between the heater and the substrate. The powder processed ceramic targets were prepared according to a description published previously [5]. The ablation target chosen for this work was $Ba_{0.6}Sr_{0.4}TiO_3$.

The RBS technique used involved the acceleration of He^+ ions to 2 MeV by a National Electrostatics Corporation (NEC) tandem pelletron accelerator. This He^+ ion beam is collimated to a 1 mm diameter beam which is incident upon the crystal / film. The scattered helium ions were detected at a backscattering angle of 170^0 with a surface barrier detector. The energy resolution of the detection system is 20 KeV to 25 KeV. The (001) channeled spectra were obtained by rotating the samples about the beam axis (ϕ) and perpendicular to it (θ), until a minimum yield was located. The minima in the backscattering yield occurs when the incident beam is aligned along certain planar and/or axial symmetry directions in the crystal, i.e., channeling. When the beam is not aligned in either direction, no channeling is present and the *random* spectrum is obtained. The energy detection system is calibrated with a standard prior to data acquisition. The elements in the crystal are determined from the detected energies of the

backscattered ions which are related to the mass of the atoms. The composition of the crystals / films were obtained by utilizing the software program RUMP to fit the data [6].

The ellipsometry data was obtained using a J.A. Woollam VASE. In this system, the elliptically-polarized light produced by reflecting plane-polarized light from the surface under study is modulated by a rotating analyzer. Both the wavelength of the monochromatic incident light and the angle of incidence can be varied. At each wavelength, after 150 revolutions of the analyzer, a data acquisition program subtracts a reading obtained with the shutter closed from a reading obtained with the shutter open. During a measurement, the wavelength is scanned from 4000 Å to 8000 Å at steps of 100 Å. Two angles of incidence were examined at each spot.

RESULTS AND DISCUSSION

Analysis of the Single Crystal Substrates

RBS Results

Figures 1 and 2 show the random and channeled RBS spectra of Pr_2CuO_4 and $Pr_{2-x}Ce_xCuO_4$ single crystals. The insets show an expanded energy scale (x-axis) of the channeled spectra. The horizontal axis is proportional to the energy at which the backscattered ion was detected. The vertical axis is the normalized yield. The ratio of the elements (in atomic %) were determined by the best fit of the RUMP simulation. The ratio of the elements and the minimum yield obtained for each element are given in Table 1.

As indicated in Fig. 2, Pr and Ce atoms cannot be resolved in the RBS spectra due to similar mass; so in the simulation $x = 0.17$ for Ce is used in place of Pr in the doped specimen. This value for x was determined from the x-ray diffraction data. As seen in the figures, Pt (up to 1%) is incorporated into the crystal through contamination by the crucible. It should be noted that Pt is seen to exhibit channelling behavior which can be observed by the definite appearance of a sharp peak and a low minimum yield in the channeled spectra. This indicates that Pt is in substitutional sites. It is assumed that Pt substitutes for Cu in the specimen, as was seen in a previous report [7]; where substitution causes the critical temperature, T_c, to decrease.

Table 1. Elemental Proportions (Atomic%) and Minimum Yields (%) Obtained from the Best RUMP Fit to the RBS Data for Pr_2CuO_4 and $Pr_{2-x}Ce_xCuO_4$.

Sample	Pr (%), Min. Yield (%)	Ce(%), Min. Yield (%)	Cu(%), Min. Yield (%)	O(%), Min. Yield (%)	Pt(%), Min. Yield (%)
Pr_2CuO_4	29.0, 5	N/A N/A	12.0, 5	58.0 N/A	1.0 5
$Pr_{2-x}Ce_xCuO_4$	22.1, 4	4.5, 4	14.4, 40	58.4, N/A	0.6, 40

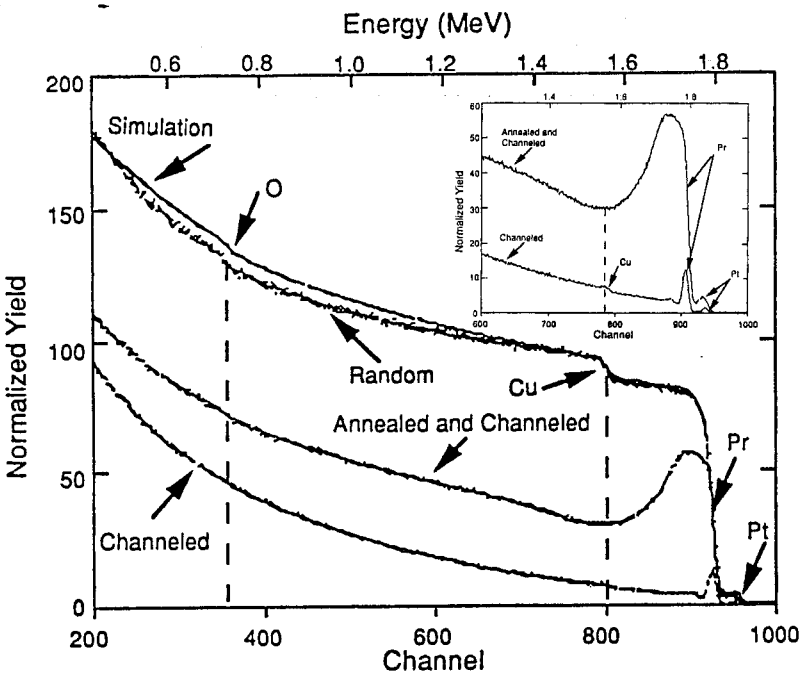

Figure 1. Random and channeled RBS spectra and simulation obtained from a fit to data for Pr_2CuO_4. Inset shows expanded energy scale (x-axis) for the channeled spectra.

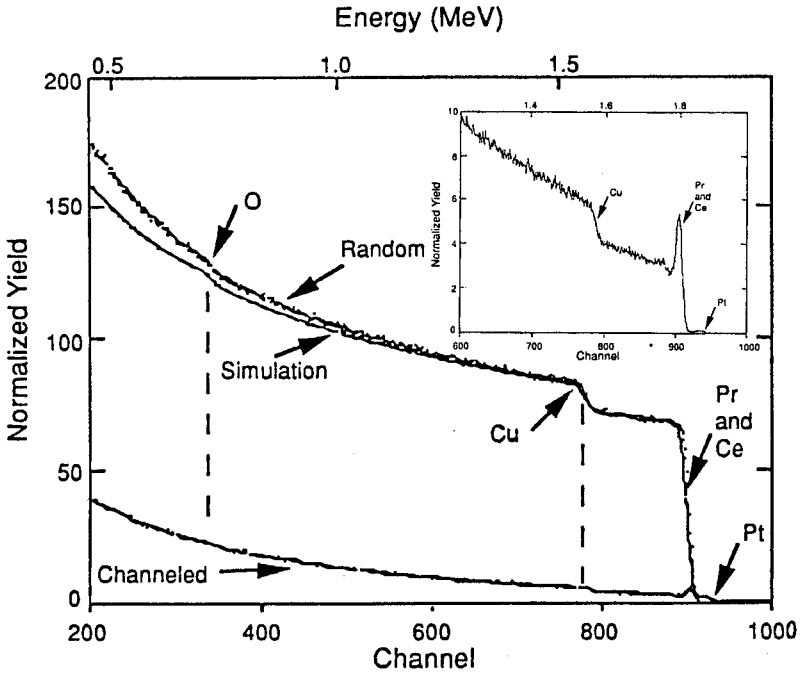

Figure 2. Random and channeled RBS spectra and simulation obtained from a fit to data for $Pr_{2-x}Ce_xCuO_4$. Inset shows expanded energy scale (x-axis) for the channeled spectra.

In general, the minimum yield obtained for the elements, as seen in Table 1, is very low indicating the crystal is well-oriented and the crystalline structure is very well-ordered. As shown in the figures, most elements appear predominantly substitutional since channeling occurs for all elements in both crystals. However, as shown in Figure 2 (inset), for the $Pr_{2-x}Ce_xCuO_4$ sample, Cu/Pt do not channel as well as indicated by their higher yields. Since both Cu and Pt appear to channel relatively poorly in this specimen, it is consistent with Pt substituting for Cu in the material. Also, the poor channeling may indicate that Cu/Pt are slightly displaced from their lattice sites. Previous workers have noticed a bending of Cu-O chains upon doping in the material [8]. The Ce doping may also cause this distortion in the crystal. The channeled spectrum for the annealed Pr_2CuO_4 sample is shown in Figure 1. As shown in the figure, the minimum yield for the Pr has increased to ~ 30%. However, the yield is not as high as for a random spectrum. This implies some disorder, from the creation of oxygen vacancies and/or surface realignment. Also, the back ledge of the spectrum does not have as low a yield as the unannealed sample. This could be due to the presence of oxygen vacancies throughout the sample or from dechanneling from the disordered surface.

VASE Results

In Figs. 3 and 4, the VASE spectra of the imaginary part of the dielectric function for both Pr_2CuO_4 and the $Pr_{2-x}Ce_xCuO_4$ are shown. As shown in Fig. 3, an absorption peak appears at 1.5 eV (at 8000 Å). This absorption peak has been assigned to a bound charge transfer excitation from the Cu(3d) to O(2p) in the Cu oxygen plane [9,10]. The sharpness of the transition may be due to the lack of a decay channel for the excited carrier [7]. In Figure 4, which shows the VASE spectrum of the $Pr_{2-x}Ce_xCuO_4$ specimen, the material becomes conducting upon doping with Ce, the 1.5 eV transition is suppressed from the introduction of free-carriers which act to produce screening of the Cu oxygen planes. In Fig. 5, the VASE spectrum of the imaginary part of the dielectric function of the annealed Pr_2CuO_4 sample is shown. The oscillator strength for the transition is decreased (transition is weakened) and it is shifted downward in energy. The weakening and downward shift of the peak may be caused by the opening of a decay channel for the carrier. The decay channel may be viewed as disorder in the material as also observed in the RBS data.

Analysis of the Films and Film / Substrate Interfaces

SEM / EDS Results

The SEM micrograph of the surface of the BSTO film on the Pr_2CuO_4 substrate is shown in Fig. 6. As shown in the figure, the film surface is fairly uniform. However, particulates are evident on the surface. EDS was performed on the particulates, and results show that the particulates consist of Ba, Sr, Ti, and O. Pr and Cu are also present. It is apparent from the compositional analysis, that the particulates have been expelled from the target. Also as noted above, the compositional analysis of the film reveals the elements from the target and from the substrate. The nominal thickness of the film was measured by a Dektak profilometer to be 3000 Å which made it transparent to the electron beam. The EDS analysis of the BSTO film deposited on $Pr_{2-x}Ce_xCuO_4$ specimen also revealed Ba, Sr, Ti and O as well as Pr, Ce, and Cu.

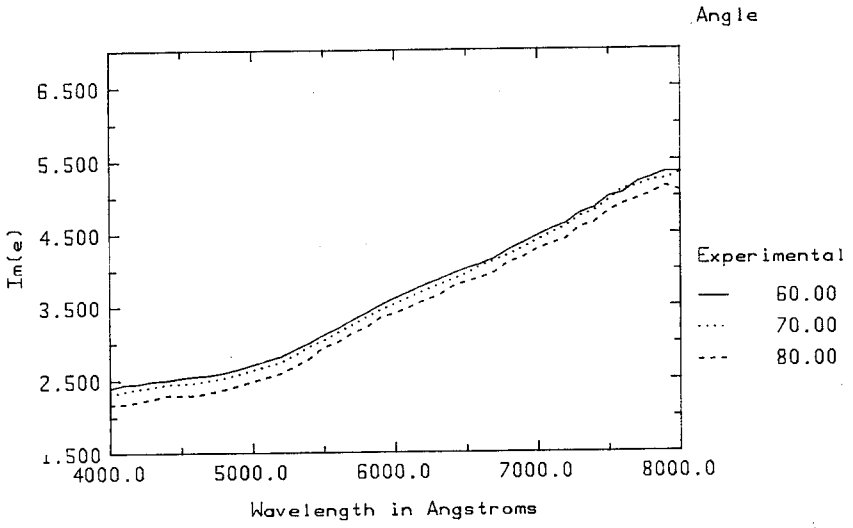

Figure 3. VASE spectrum of the imaginary part of the dielectric function versus wavelength for the Pr_2CuO_4 sample, $\theta = 60^0$, 70^0 and 80^0.

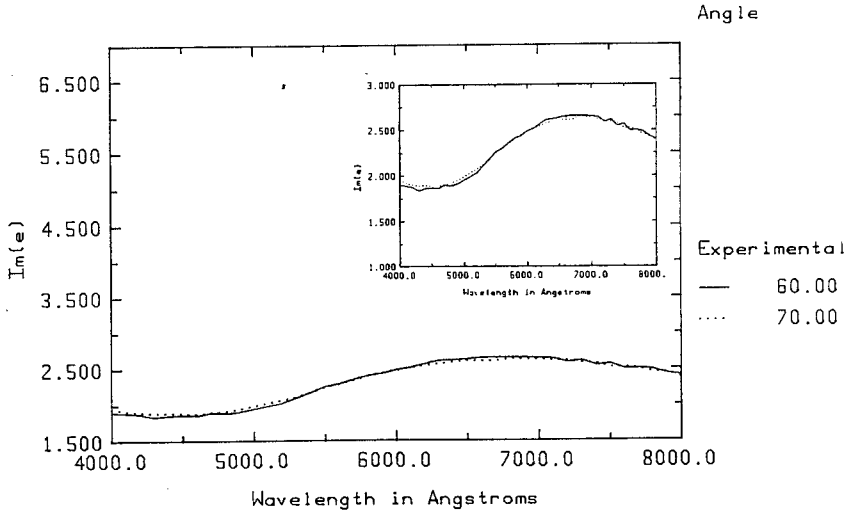

Figure 4. VASE spectrum of the imaginary part of the dielectric function versus wavelength for the $Pr_{2-x}Ce_xCuO_4$ sample, $\theta = 60^0$ and 70^0, (inset shows an expanded y-scale of the sample).

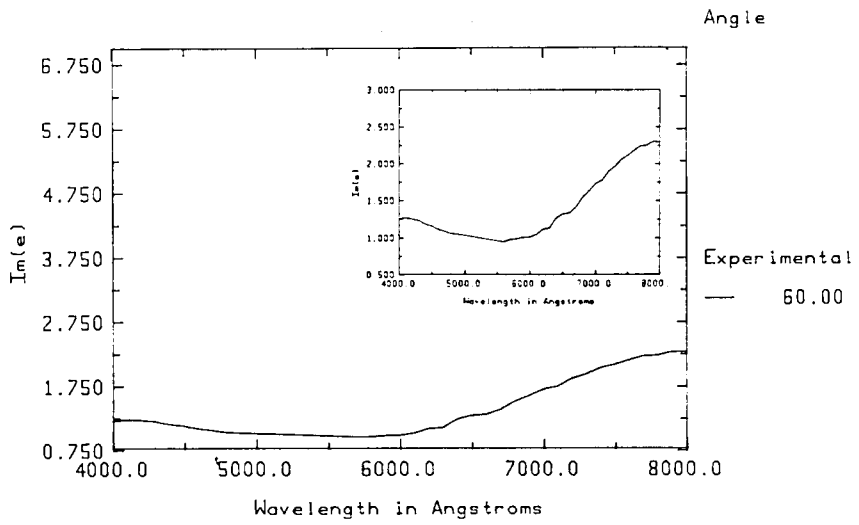

Figure 5. VASE spectrum of the imaginary part of the dielectric function versus wavelength for the annealed Pr_2CuO_4 sample, (inset shows an expanded y-scale of the sample), $\theta = 60^0$. .

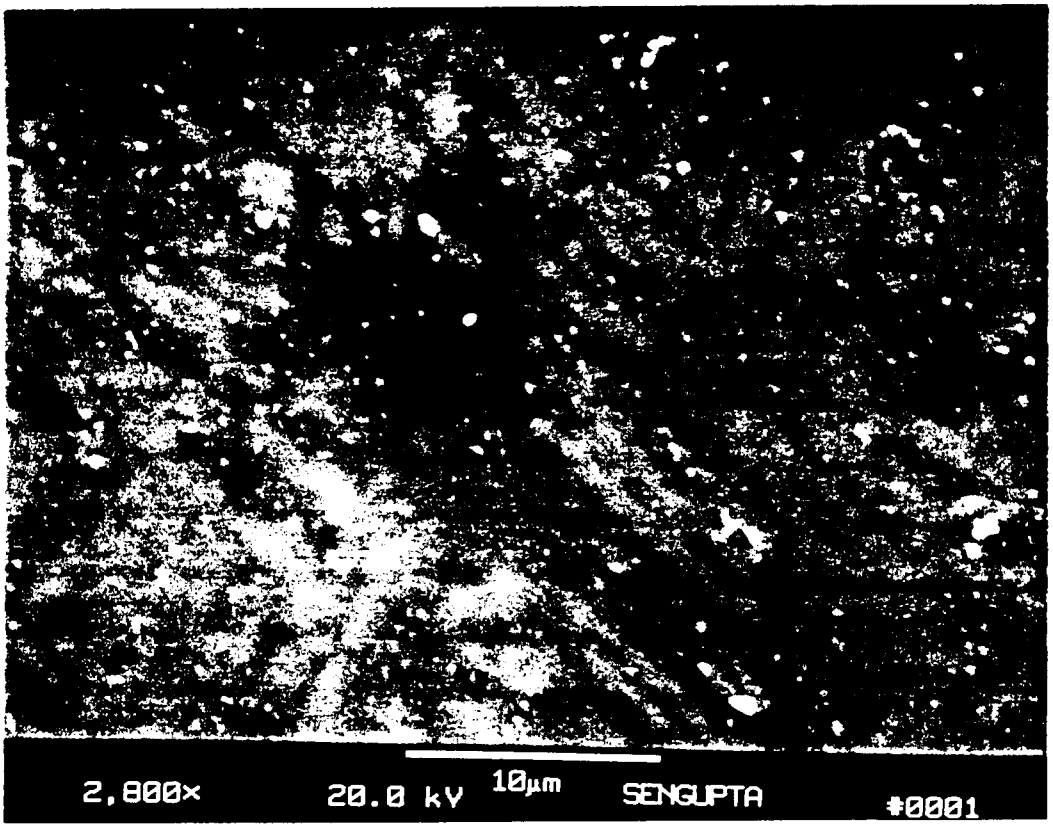

Figure 6. SEM micrograph of the $Ba_{0.6}Sr_{0.4}TiO_3$ film deposited on Pr_2CuO_4 single crystal substrate.

RBS Results

The RBS spectrum for the BSTO film on the Pr_2CuO_4 substrate is shown in Fig. 7. The dotted line is the measured data for the RBS spectra and the solid line is the RUMP fit to the data. As shown in the Fig. 8, this fit was done by subtracting the measured RBS spectra for the Pr_2CuO_4 single crystal and by adding the stoichiometrically correct peaks for Ba, Sr, and Ti. Therefore, it is evident from the fit to the data, that the film that was deposited was stoichiometrically identical to the target, which is Ba = 0.60, Sr = 0.40, and Ti = 1.03 , and O = 3.0.

However, as shown in Fig. 9, the simulated spectrum does not show a good fit to the RBS spectrum of the BSTO film (inset shows the expected positions for Ba, Sr, and Ti) on Ce doped Pr_2CuO_4. This may be attributed to the poor surface quality of the substrate. As observed for the substrate, from the RBS data, it is apparent that the crystal has a oxygen rich and disordered surface as indicated by the poor channeling for Cu/Pt sites. Therefore the front part of the spectrum is seen to slope downward or "roll-off". Therefore, the RBS data cannot be used to make any conclusive analysis of the film deposited on this substrate.

Glancing Angle X-ray Diffraction

The glancing angle x-ray diffraction data for the BSTO film deposited on Pr_2CuO_4 is shown in Fig. 10 (inset shows the x-ray diffraction pattern for the $Ba_{0.6}Sr_{0.4}TiO_3$ target material). A rotating anode x-ray unit emitting Cu-Kα (1.5415 Å) emission was used as the source. The x-ray beam was incident on the sample at an angle of 1 degree to the surface of the film. The x-ray pattern matches closely to that for $Ba_{0.6}Sr_{0.4}TiO_3$. The *hkl* values for these peaks are indicated on the figure. However, another phase is also present in the film. This phase corresponds to $Ba_{0.91}Sr_{0.09}TiO_4$ and the x-ray peaks for this phase are indicated on the figure by an asterisk.

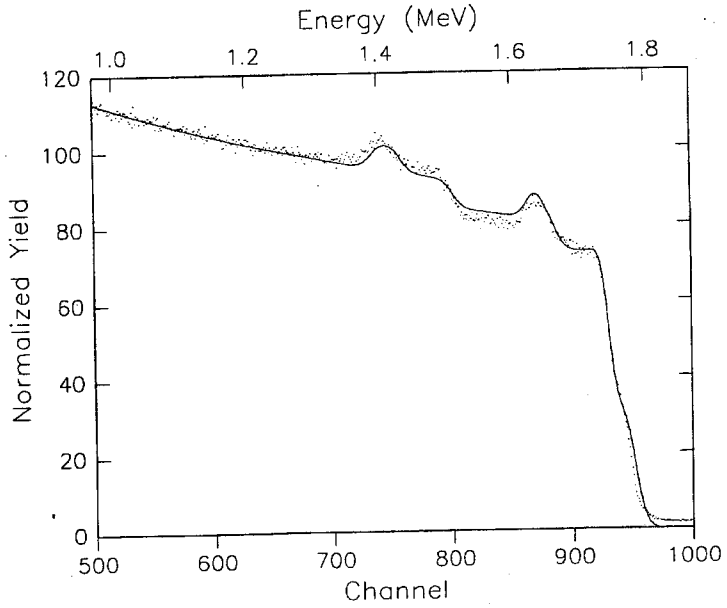

Figure 7. RBS spectrum for the BSTO/Pr_2CuO_4 sample (dotted line) and a fit to the data (solid line) obtained from the measured data for the Pr_2CuO_4 substrate and the film containing $Ba_{0.6}Sr_{0.4}TiO_3$.

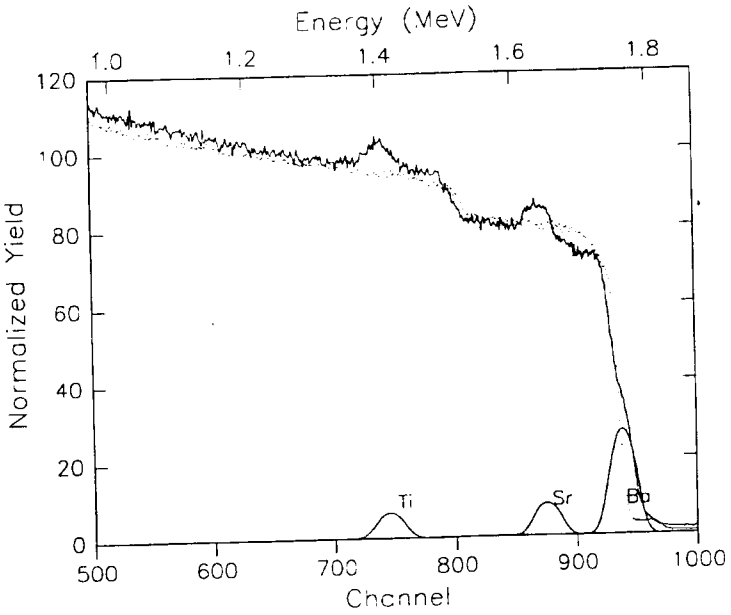

Figure 8. RBS spectrum for the BSTO / Pr_2CuO_4 sample (solid line) and the RBS spectrum for the Pr_2CuO_4 crystal (dotted line) and the corresponding peaks for Ba, Sr, and Ti.

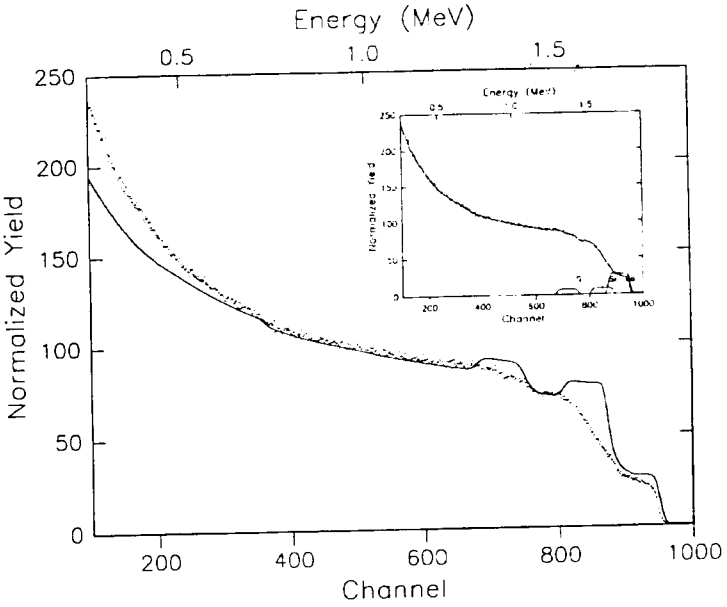

Figure 9. RBS spectrum for the BSTO / $Pr_{2-x}Ce_xCuO_4$ sample (dotted line) and a fit to the data (solid line), (inset shows the expected position of the Ba, Sr, and Ti peaks).

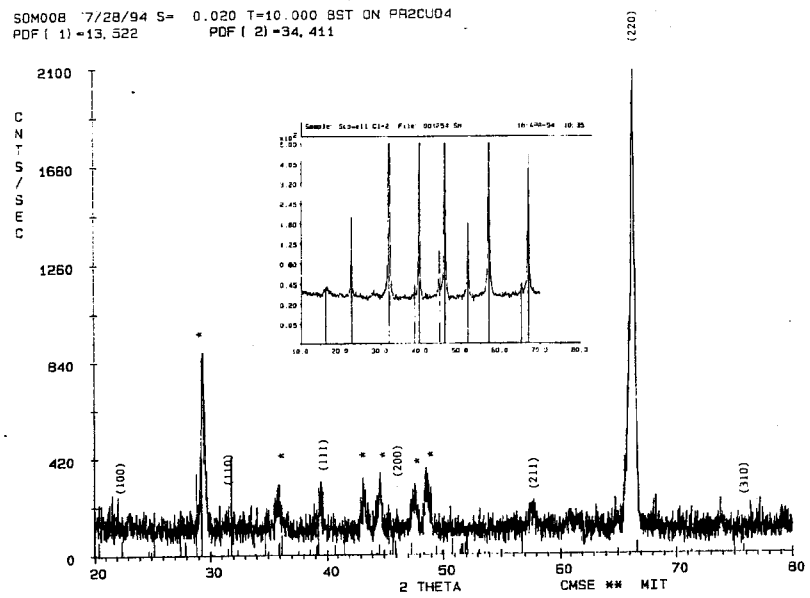

Figure 10. Glancing Angle X-ray Diffraction pattern for BSTO deposited on Pr_2CuO_4 (inset shows the x-ray diffraction pattern for the $Ba_{0.6}Sr_{0.4}TiO_3$ target material).

As shown in the inset the target material does not contain this secondary phase and it is not observed when the films are deposited on other substrates. The presence of this phase may be attributed to the film-substrate interaction, possibly due to the presence of surface disorder (oxygen vacancies) as indicated by the RBS and VASE data of the substrate. Further investigations on this specimen are currently being done.

CONCLUSION

The crystal structures and composition of the cuprate crystals were investigated using RBS with ion beam channeling. The minimum yields obtained for the elements in the crystals indicate that the crystals are well-oriented and very ordered. The addition of Cerium to the material causes a slight displacement of Cu from its normal lattice site. Also, Pt was included in the crystals due to the contamination from the crucible. The spectrum of the annealed crystal shows disorder which was confirmed by RBS and VASE data.

The RBS spectrum of the laser ablated BSTO / Pr_2CuO_4 film indicated similar film and target compositions. However, the presence of a barium rich secondary phase ($Ba_{0.91}Sr_{0.09}TiO_4$) was evident from x-ray studies. This phase may have been created due to the presence of the oxygen vacancies present in the substrate due to annealing. The RBS data of the BSTO / $Pr_{2-x}Ce_xCuO_4$ sample is inconclusive due to the poor surface quality of the substrate. The incorporation of superconducting electrodes with ferroelectric materials is presently under investigation.

ACKNOWLEDGMENTS

The authors wish to thank Dr. Arlete Cassanho for the cuprate crystals and Dr.Allen Kirkpatrick of Epion Corporation, Bedford, MA for his help.

REFERENCES

[1] O. Vendik, I. Mironenko, and L. Ter-Martirosyan, *Microwaves and RF*, pp. 67-70, July 1994.
[2] S.B. Desu, *J. of Integrated Ferroelectrics*, in press (1994).
[3] A. Cassanho et.al , *J. Crystal Growth*, vol. 96, pp. 999 (1988).
[4] L.C.Sengupta, S.Sengupta, W.E.Kosik, and J.D.Demaree, *J.Cryst. Growth*, vol. 128, pp.817-823 (1993).
[5] L.C. Sengupta, S. Stowell, E. Ngo, M.E. O'Day and R. Lancto, *J. of Integrated Ferroelectrics*, in press (1994).
[6] L.R. Doolittle, *Nuclear Instru. Meth.*, vol B9, p. 334 (1985).
[7] Y. Hidaka, *Proc. of 2nd ISS '89*, T. Ishoguro and K. Kajimura, eds., Springer-Verlag, p. 229 (1990).
[8] J.M. Tarascon, et. al., *Phys. Rev. B*, vol. 40, p. 4494 (1989).
[9] S. Tajima, et. al., *J. Opt. Soc. Am.*, vol. B6, p.475 (1989).
[10] M.K. Kelly, P. Barboux, J.M. Tarascon, and D.E. Aspnes, *Phys. Rev. B*, vol. 40, p.6747 (1989).

DISTRIBUTION LIST

No. of Copies	To
1	Office of the Under Secretary of Defense for Research and Engineering, The Pentagon, Washington, DC 20301
	Director, U.S. Army Research Laboratory, 2800 Powder Mill Road, Adelphi, MD 20783-1197
1	ATTN: AMSRL-OP-SD-TP, Technical Publishing Branch
1	AMSRL-OP-SD-TA, Records Management Administrator
	Director, U.S. Army Research Laboratory, 2800 Powder Mill Road, Adelphi, MD 20783-1197
1	ATTN: Technical Library
	Commander, Defense Technical Information Center, Cameron Station, Building 5, 5010 Duke Street, Alexandria, VA 23304-6145
2	ATTN: DTIC-FDAC
1	MIA/CINDAS, Purdue University, 2595 Yeager Road, West Lafayette, IN 47905
	Commander, Army Research Office, P.O. Box 12211, Research Triangle Park, NC 27709-2211
1	ATTN: Information Processing Office
	Commander, U.S. Army Materiel Command, 5001 Eisenhower Avenue, Alexandria, VA 22333
1	ATTN: AMCSCI
	Commander, U.S. Army Materiel Systems Analysis Activity, Aberdeen Proving Ground, MD 21005
1	ATTN: AMXSY-MP, H. Cohen
	Commander, U.S. Army Missile Command, Redstone Arsenal, AL 35809
1	ATTN: AMSMI-RD-CS-R/Doc
	Commander, U.S. Army Armament, Munitions and Chemical Command, Dover, NJ 07801
2	ATTN: Technical Library
	Commander, U.S. Army Natick Research, Development and Engineering Center, Natick, MA 01760-5010
1	ATTN: DFAS-IN-EM-TL, Technical Library
	Commander, U.S. Army Satellite Communications Agency, Fort Monmouth, NJ 07703
1	ATTN: Technical Document Center
	Commander, U.S. Army Tank-Automotive Command, Warren, MI 48397-5000
1	ATTN: AMSTA-ZSK
1	AMSTA-TSL, Technical Library
	Commander, White Sands Missile Range, NM 88002
1	ATTN: STEWS-WS-VT
	President, Airborne, Electronics and Special Warfare Board, Fort Bragg, NC 28307
1	ATTN: Library

No. of Copies	To
	Director, U.S. Army Research Laboratory, Weapons Technology, Aberdeen Proving Ground, MD 21005-5066
1	ATTN: AMSRL-WT
	Commander, Dugway Proving Ground, UT 84022
1	ATTN: Technical Library, Technical Information Division
	Commander, U.S. Army Research Laboratory, 2800 Powder Mill Road, Adelphi, MD 20783
1	ATTN: AMSRL-SS
	Director, Benet Weapons Laboratory, LCWSL, USA AMCCOM, Watervliet, NY 12189
1	ATTN: AMSMC-LCB-TL
1	AMSMC-LCB-R
1	AMSMC-LCB-RM
1	AMSMC-LCB-RP
	Commander, U.S. Army Foreign Science and Technology Center, 220 7th Street, N.E., Charlottesville, VA 22901-5396
3	ATTN: AIFRTC, Applied Technologies Branch, Gerald Schlesinger
	Commander, U.S. Army Aeromedical Research Unit, P.O. Box 577, Fort Rucker, AL 36360
1	ATTN: Technical Library
	U.S. Army Aviation Training Library, Fort Rucker, AL 36360
1	ATTN: Building 5906-5907
	Commander, U.S. Army Agency for Aviation Safety, Fort Rucker, AL 36362
1	ATTN: Technical Library
	Commander, Clarke Engineer School Library, 3202 Nebraska Ave., N, Fort Leonard Wood, MO 65473-5000
1	ATTN: Library
	Commander, U.S. Army Engineer Waterways Experiment Station, P.O. Box 631, Vicksburg, MS 39180
1	ATTN: Research Center Library
	Commandant, U.S. Army Quartermaster School, Fort Lee, VA 23801
1	ATTN: Quartermaster School Library
	Naval Research Laboratory, Washington, DC 20375
2	ATTN: Dr. G. R. Yoder - Code 6384
	Chief of Naval Research, Arlington, VA 22217
1	ATTN: Code 471
	Commander, U.S. Air Force Wright Research & Development Center, Wright-Patterson Air Force Base, OH 45433-6523
1	ATTN: WRDC/MLLP, M. Forney, Jr.
1	WRDC/MLBC, Mr. Stanley Schulman

No. of Copies	To
	U.S. Department of Commerce, National Institute of Standards and Technology, Gaithersburg, MD 20899
1	ATTN: Stephen M. Hsu, Chief, Ceramics Division, Institute for Materials Science and Engineering
1	Committee on Marine Structures, Marine Board, National Research Council, 2101 Constitution Avenue, N.W., Washington, DC 20418
1	Materials Sciences Corporation, Suite 250, 500 Office Center Drive, Fort Washington, PA 19034
1	Charles Stark Draper Laboratory, 555 Technology Square, Cambridge, MA 02139
	Wyman-Gordon Company, P.O. Box 8001, North Grafton, MA 01536-8001
1	ATTN: Technical Library
	General Dynamics, Convair Aerospace Division, P.O. Box 748, Fort Worth, TX 76101
1	ATTN: Mfg. Engineering Technical Library
	Plastics Technical Evaluation Center, PLASTEC, ARDEC, Bldg. 355N, Picatinny Arsenal, NJ 07806-5000
1	ATTN: Harry Pebly
1	Department of the Army, Aerostructures Directorate, MS-266, U.S. Army Aviation R&T Activity - AVSCOM, Langley Research Center, Hampton, VA 23665-5225
1	NASA - Langley Research Center, Hampton, VA 23665-5225
	U.S. Army Vehicle Propulsion Directorate, NASA Lewis Research Center, 2100 Brookpark Road, Cleveland, OH 44135-3191
1	ATTN: AMSRL-VP
	Director, Defense Intelligence Agency, Washington, DC 20340-6053
1	ATTN: ODT-5A (Mr. Frank Jaeger)
	U.S. Army Communications and Electronics Command, Fort Monmouth, NJ 07703
1	ATTN: Technical Library
	U.S. Army Communications and Electronics Command, Intelligence and Electronic Warfare Center, Fort Monmouth, NJ 07703-5211
1	ATTN: Frank Elmer, AMSEL-RD-IEW-TAE-M
	U.S. Army Research Laboratory, Electronic Power Sources Directorate, Fort Monmouth, NJ 07703
1	ATTN: AMSRL-EP-M, W. C. Drach
1	AMSRL-EP-M, T. E. Koscica
1	AMSRL-EP-M, R. W. Babbit
	Director, U.S. Army Research Laboratory, Watertown, MA 02172-0001
2	ATTN: AMSRL-OP-WT-IS, Technical Library
20	Authors